BIOCHEMISTRY
including biophysical chemistry & molecular biology
Article

Biochemistry **2010,** *49,* 6375–6385 6375
DOI: 10.1021/bi100381y

Kinetic Mechanism of the Rtt109−Vps75 Histone Acetyltransferase−Chaperone Complex†

Brittany N. Albaugh, Erin M. Kolonko, and John M. Denu*

Department of Biomolecular Chemistry, University of Wisconsin, 1300 University Avenue, Madison, Wisconsin 53706

Received March 11, 2010; Revised Manuscript Received June 18, 2010

ABSTRACT: Rtt109 is a histone acetyltransferase (HAT) involved in promoting genomic stability, DNA repair, and transcriptional regulation. Rtt109 associates with the NAP1 family histone chaperone Vps75 and stimulates histone acetylation. Here we explore the mechanism of histone acetylation and report a detailed kinetic investigation of the Rtt109−Vps75 complex. Rtt109 and Vps75 form a stable complex with nanomolar binding affinity (K_d = 10 ± 2 nM). Steady-state kinetic analysis reveals evidence of a sequential kinetic mechanism whereby the Rtt109−Vps75 complex, AcCoA, and histone H3 substrates form a complex prior to chemical catalysis. Product inhibition studies demonstrate that CoA binds competitively with AcCoA, and equilibrium measurements reveal AcCoA or CoA binding is not stimulated in the presence of H3 substrate. Additionally, the Rtt109−Vps75 complex binds H3 substrates in the absence AcCoA. Pre-steady-state kinetic analysis suggests the chemical attack of substrate lysine on the bound AcCoA is the rate-limiting step of catalysis, while the pH profile of k_{cat} reveals a critical ionization with a pK_a of 8.5 that must be unprotonated for catalysis. Amino acid substitution at D287 and D288 did not substantially change the shape of the k_{cat}−pH profile, suggesting these conserved residues do not function as base catalysts for histone acetylation. However, the D288N mutant revealed a dramatic 1000-fold decrease in k_{cat}/K_m for AcCoA, consistent with a role in AcCoA binding. Together, these data support a sequential mechanism in which AcCoA and H3 bind to the Rtt109−Vps75 complex without obligate order, followed by the direct attack of the unprotonated ε-amino group on AcCoA, transferring the acetyl group to H3 lysine residues.

In eukaryotes, DNA is wrapped around an octamer of histones to form the fundamental unit of chromatin called the nucleosome. Post-translational modification of histones elicits effects on chromatin compaction, transcriptional control, and replication modulation (*1*, *2*). Lysine 56 (K56), a residue located within the globular fold of histone H3, is abundantly acetylated in *Saccharomyces cerevisiae* and *Schizosaccharomyces pombe* (*3*−*6*). During replication-coupled nucleosome assembly, newly synthesized H3 molecules are marked with K56ac (lysine 56 acetylation), subsequently assembled into DNA to form chromatin, and then deacetylated in G2/M phase by the NAD-dependent activities of the sirtuin homologues Hst3[1] and Hst4 (*5*, *7*, *8*). Furthermore, K56ac predominates with exposure to DNA damage reagents, implicating a role for K56ac in genomic integrity and DNA repair (*6*, *9*−*11*). Specifically, K56ac is required for chromatin reassembly after double-stranded DNA breaks, signals for the completion of DNA repair, and increases the stability of replication forks (*10*, *11*). Replication-independent roles for K56 modification exist, as this acetylation and enhanced histone turnover are prominent at active gene promoters, while the hypoacetylation of K56 marks regions of silent chromatin such as telomeres (*12*, *13*). In mammals, the level of K56ac is elevated in response to DNA damage and is enriched in cancerous cell lines, suggesting that roles for K56ac are conserved (*14*). K56ac is also associated with genes bound by key regulators of pluripotency in embryonic stem cells, suggesting this histone modification is an epigenetic marker for the pluripotent state (*15*).

One particular family of proteins that bind histones and mediate chromatin dynamics consists of histone chaperones. Previously presumed only to function in preventing nonspecific interactions of histones, these chaperones are now recognized as important regulators of histone assembly and nucleosome eviction (*16*). For example, the histone chaperone Asf1 is required for K56ac in replication-coupled nucleosome assembly upstream of the actions of histone chaperones CAF-1 and Rtt106 (*17*). Asf1 also increases the rate of histone turnover in nonreplicative processes such as transcriptional activation at gene promoters (*12*). Vps75 is a NAP (nucleosome assembly protein) histone chaperone homologue involved in transcription-related histone exchange and in stimulating the Rtt109-dependent acetylation of H3 tail residues (*11*, *18*−*20*).

Recently, the yeast protein Rtt109 was discovered as a novel lysine acetyltransferase (KAT11) that associates with histone chaperones and utilizes AcCoA to acetylate K56 of H3 (eq I) (*5*, *6*, *11*, *21*).

$$\text{AcCoA} + \text{H3} \Leftrightarrow \text{Ac}-\text{H3} + \text{CoA} \qquad \text{(I)}$$

†This work supported by National Institutes of Health Grant GM059785 and a postdoctoral fellowship (E.M.K.) from the American Heart Association (0920041G).

*To whom correspondence should be addressed: University of Wisconsin School of Medicine and Public Health, 551 Medical Sciences Center, 1300 University Ave., Madison, WI 53706. E-mail: jmdenu@wisc.edu. Phone: (608) 265-1859. Fax: (608) 262-5253.

[1]Abbreviations: HAT, histone acetyltransferase; DTT, dithiothreitol; Rtt109 and Rtt106, regulators of Ty1 transposition 109 and 106, respectively; CAF-1, chromatin assembly factor 1; Vps75, vacuolar protein sorting 75; Asf1, anti-silencing function 1; Hst3 and Hst4, homologues of SIR two 3 and 4, respectively; SDS−PAGE, sodium dodecyl sulfate−polyacrylamide gel electrophoresis; Esa1, essential Sas2-related acetyltransferase 1; PCAF, p300/CBP-associated factor; LC−MS, liquid chromatography−mass spectrometry; AcCoA, acetyl-coenzyme A; CoA, coenzyme A.

Published on Web 06/18/2010

Interestingly, Rtt109 shares no sequence homology with other mammalian HATs (histone acetyltransferases), although recently reported crystal structures reveal Rtt109 is structurally similar to mammalian HAT p300 (KAT3) (*21*−*25*). Unlike other HATs, Rtt109 requires association with a histone chaperone, Asf1 or Vps75, for catalytic activation (*11*, *19*). In vivo, *asf1*Δ results in the loss of K56ac and K9ac while *vps75*Δ diminishes the levels of K9ac and K23ac with little change in the level of K56ac (*6*, *11*, *26*−*28*). In association with Asf1, Rtt109 acetylates H3K56 in vitro, but only in the presence of histone H4 (*11*). In contrast, the high-affinity Rtt109−Vps75 complex (Rtt109−Vps75) demonstrates broader substrate specificity and acetylates K56, K9, K14, and K23 on H3 alone, H3−H4, and H3 tail peptides (*11*, *26*). While the Asf1−Rtt109 complex is responsible for K56ac and a portion of K9ac in vivo, Rtt109−Vps75 appears to function as an H3 tail acetyltransferase, although how Rtt109−Vps75 directs the fate of histones at specific chromatin regions is not fully understood (*11*, *18*, *26*, *28*). Together, these data suggest distinct pathways for the regulation of Rtt109 by histone chaperones.

Recently, Rtt109 was demonstrated to be essential for the pathogenesis of *Candida albicans*, the primary fungal genus (*Candida*) responsible for opportunistic human infections (*29*). Loss of Rtt109 in *C. albicans* results in increased sensitivity to genotoxic agents, diminished pathogenicity in mice, and greater susceptibility to ROS-mediated cell death by macrophages (*29*). Given *C. albicans* poses a persistent public health problem and resistance to the current classes of antifungal agents is widespread, Rtt109 may be a novel therapeutic target in the treatment of fungal infections (*30*). Because Rtt109 is uniquely regulated by histone chaperones and the importance of developing new mechanism-based inhibitors for antifungal therapy, we sought to elucidate the catalytic mechanism of yeast Rtt109−Vps75. In this study, we have determined the binding affinity of Vps75 for Rtt109, elucidated the kinetic mechanism of Rtt109−Vps75, established the order of substrate binding, and identified the rate-limiting step of the catalytic cycle. With various biochemical methods such as steady-state kinetic analysis, pre-steady-state methods, pH−rate profile analysis, and various binding assays, the results are consistent with a random sequential mechanism with rate-limiting chemical catalysis that is characterized by the direct attack of an unprotonated histone lysine on enzyme-bound AcCoA.

EXPERIMENTAL PROCEDURES

Chemicals and Reagents. AcCoA, CoA, DTT, pyruvate dehydrogenase, pyruvic acid, and NAD^+ were purchased from Sigma-Aldrich. Tris-HCl, P81 cellulose discs, and sodium chloride were available from Fisher. Most other reagents were of the highest grade available and purchased from either Fisher or Sigma-Aldrich. [^{3}H]Acetyl-CoA (2−25 Ci/mmol) was obtained from Morevek, and acrylamide/bisacrylamide was purchased from Bio-Rad. Site-directed mutagenesis kits from Stratagene were utilized to introduce point mutations at D287 and D288 of Rtt109.

Expression, Purification, and Quantification of Proteins. Expression and purification of the coexpressed recombinant His-Vps75−untagged Rtt109 complex and His-Vps75 were performed as detailed by Berndsen et al. (*26*). Untagged Rtt109 was further purified by separation of the complex via an HP-Phenyl Sepharose column (GE) followed by purification over a Superdex 200 sizing column (GE), or a His-tagged construct of Rtt109 was purified by nickel affinity purification. These proteins freely exchange and do not form an irreversible complex. The same k_{cat} was achieved whether experiments were performed with (His-tagged or untagged) Rtt109 and Vps75 added as separate components or with copurified Rtt109−Vps75. H3 protein and H4 protein from *Xenopus laevis* were recombinantly purified as previously described by Luger et al. (*31*). Rtt109 and Vps75 proteins were quantified by one of two methods: Bradford reagent assay or densitometry analysis using bovine serum albumin as the protein standard and Coomassie Blue R250 as the protein stain. Concentrations of copurified Rtt109−Vps75 were determined via densitometry of Rtt109, as Vps75 was present in an ∼2-fold excess. These concentrations were confirmed by amino acid analysis performed by the University of California-Davis Proteomics Core Facility. H3 protein was quantified by determining the absorbance at 276 nm using an extinction coefficient (ε) of 4040 M^{-1} cm^{-1}. H3−H4 was reconstituted as previously described by Tanaka et al. (*32*).

Synthesis and Analysis of the H3 Peptide. The utilization of the whole H3 protein substrate was problematic in some assays because of either the high acetylation background activity of H3 or protein precipitation caused when H3 and Rtt109−Vps75 were combined at high concentrations. Because an H3 tail peptide has previously been shown to be a substrate for Rtt109−Vps75, the peptide substrate was utilized to circumvent the issues of using full-length H3 (*26*). The H3 peptide (amino acid sequence ARTKQTARKSTGGKAPRKQL) was generated by the University of Wisconsin-Madison Biotechnology Center (UWBC) and purified over a preparative C18 HPLC column. Mass spectrometric identification of the peptide was performed on a Bruker REFLEX II:MALDI-TOF (matrix-assisted laser desorption ionization time-of-flight) instrument. The chromatographic purity of the purified peptide was found to be ≥95%, and the peptide concentration was determined by amino acid analysis by the University of California-Davis Proteomics Core Facility.

Fluorescein Labeling of Vps75 and Fluorescence Polarization Measurements. Vps75 was labeled with fluorescein 5-maleimide (Invitrogen) according to the manufacturer's procedures in PBS (phosphate-buffered saline) and resulted in 1:1 ratio of label to Vps75, suggesting that one of two cysteines in Vps75 was preferentially labeled. Excess fluorescein 5-maleimide was dialyzed away (PBS) from labeled Vps75, and protein concentrations were quantified as described above. HAT activity assays with labeled Vps75 showed a <2-fold loss of activity, indicating that the labeling procedure did not appreciably hinder the ability of Vps75 to activate Rtt109. For the fluorescence polarization studies, 125 μL samples of 3.2 nM labeled $Vps75_{dimer}$ (assumed as a nondissociating dimer) and 3.7−190 nM Rtt109 in PBS containing 0.2 mM AcCoA and 0.1 mg/mL BSA were prepared and equilibrated at 25 °C for 15 min, prior to measurements being taken using a Beacon 2000 Fluorescence Polarization System. The fluorescence polarizations measurements were performed in the presence of AcCoA, as Rtt109 alone (without AcCoA or Vps75) is unstable and precipitates at 25 °C. Control experiments using BSA as the titrant showed no change in the FP signal. The fraction of bound labeled Vps75 (fraction of Rtt109−Vps75 formed) was determined by the following equation:

$$\text{fraction bound} = \frac{A_{obs} - A_f}{A_b - A_f} \quad (1)$$

where A_{obs} is the observed anisotropy, A_f is the anisotropy of free labeled $Vps75_{dimer}$, and A_b is the anisotropy of maximally bound labeled $Vps75_{dimer}$ with Rtt109. The concentration of bound complex was calculated by multiplying the fraction bound by the

$Vps75_{dimer}$ concentration used in the experiment. The total Rtt109 concentration was plotted against that of Rtt109−Vps75 (bound, labeled $Vps75_{dimer}$) and fitted to the following equation to yield the dissociation constant of the complex (K_d):

$$[\text{Rtt109}-\text{Vps75}_{dimer}] = \{[\text{Vps75}_T] + K_d + [\text{Rtt109}_T] - [([\text{Vps75}_T]+K_d+[\text{Rtt109}_T])^2 - 4[\text{Vps75}_T][\text{Rtt109}_T]]^{1/2}\}/2 \quad (2)$$

where $[\text{Rtt109}-\text{Vps75}_{dimer}]$ is the concentration of the complex, $[\text{Vps75}_T]$ is the total concentration of labeled $Vps75_{dimer}$, and $[\text{Rtt109}_T]$ is the total concentration of Rtt109. Seven separate binding trials were performed in replicate, with K_d representing the average of the trials and the standard error reported.

Histone Acetyltransferase Assays for Rtt109−Vps75. Rtt109−Vps75 histone acetyltransferase activity was monitored by one of two methods at 25 °C. In a continuous assay, Rtt109−Vps75 histone acetyltransferase activity was monitored by a coupled pyruvate dehydrogenase assay that recycles AcCoA (*33*, *34*). Briefly, CoA generated by the HAT reaction was converted to AcCoA by the pyruvate dehydrogenase complex in the presence of thiamine pyrophosphate (TPP), pyruvate, and NAD^+. Reduction of NAD^+ to NADH was monitored continuously at A_{340} using a Multiskan Ascent microplate reader to determine the initial rate of the reaction. In a discontinuous method, HAT assay components (enzyme, H3 substrate, and [^{3}H]AcCoA) were mixed and spotted at various time points on P81 phosphocellulose disks as described previously (*34*). Disks were washed with 3 × 500 mL for 5 min in 50 mM sodium bicarbonate solution (pH 9.0) and dried to remove unreacted AcCoA prior to liquid scintillation counting. An unwashed disk served to allow for the measurement of AcCoA specific activity. Minimally, two trials were performed ($n \geq 2$) in duplicate for all kinetic measurements, with error bars of data points representing the standard deviation. The standard error of each kinetic constant was determined. Each assay condition was empirically tested to ensure sufficient Vps75 was present so that ≥98% Rtt109 was maximally activated.

Bisubstrate Kinetic Measurements. The bisubstrate analysis measurements were performed in 300 μL reaction mixtures containing 50 mM Tris (pH 7.5), 1 mM DTT, 0.1 μM Rtt109, 0.8 μM Vps75, 2.4 mM TPP, 0.2 mM NAD^+, 0.2 mM pyruvate, 5 mM $MgCl_2$, and 0.05 unit/μL pyruvate dehydrogenase. The H3 peptide concentration was varied from 23 to 262 μM, and the AcCoA concentration was varied from 0.25 to 2 μM. Data were fitted to equations for a sequential mechanism (eq 3), a ping-pong mechanism (eq 4), and the equilibrium ordered mechanism (eq 5) using KinetAsyst (IntelliKinetics, State College, PA). K_a is the K_m for substrate A, K_b the K_m for substrate B, and K_{ia} the dissociation constant for substrate A. This data and all other kinetic data are shown using Kaleidagraph (Synergy Software, Reading, PA).

$$v = V_m AB/(K_{ia}K_b + K_a B + K_b A + AB) \quad (3)$$

$$v = V_m AB/(K_a B + K_b A + AB) \quad (4)$$

$$v = V_m AB/(K_a K_b + K_b A + AB) \quad (5)$$

Product Inhibition Kinetics. CoA, a product of the HAT reaction, was used as an inhibitor at varied levels of AcCoA. Using the filter binding assays, reaction conditions were employed at 50 mM Tris (pH 7.5), 1 mM DTT, 20 nM Rtt109, 0.8 μM Vps75, 50 mM NaCl, 5 μM H3 protein (approximate K_m), 0.4−14.4 μM AcCoA, and 0−600 μM CoA. The data sets were fitted to equations for competitive inhibition (eq 6), noncompetitive inhibition (eq 7), and uncompetitive inhibition (eq 8), where K_{is} is the slope inhibition constant and K_{ii} is the intercept inhibition constant:

$$v = V_m S/[K_m(1 + I/K_{is}) + S] \quad (6)$$

$$v = V_m S/[K_m(1 + I/K_{is}) + S(1 + I/K_{ii})] \quad (7)$$

$$v = V_m S/[K_m + S(1 + I/K_{ii})] \quad (8)$$

Isothermal Calorimetry of AcCoA and CoA into Rtt109−Vsp75. Isothermal calorimetry (ITC) measurements were taken using a VP-ITC microcalorimeter from MicroCal, LLC (Northampton, MA). All binding measurements were performed in 50 mM Tris (pH 7.5 and 25 °C), 5% glycerol (w/v), 50 mM NaCl, 2 mM β-mercaptoethanol, and 1 mM EDTA. Copurified Rtt109−Vps75 was dialyzed against the buffer described above, and ligand solutions were suspended in dialysis buffer. Data analysis was performed using Origin scientific plotting software, and experimental data were fit to a one-site binding model, where ΔH (enthalpy), K_a (binding constant), and n (number of binding sites) were flexible parameters. The thermodynamic parameters ΔG and ΔS were determined from the following equation:

$$\Delta G = \Delta H - T\Delta S = -RT \ln K_a \quad (9)$$

with the standard error reported. For each experiment, 37−43 automatic injections of 1−8 μL of ligand were titrated into the cell (cell volume of 1.42 mL) while the contents were being stirred at 300 rpm. AcCoA (167 μM) was titrated into 5.8 μM copurified Rtt109−Vps75. For CoA binding, 2 mM CoA was titrated into 50 μM copurified Rtt109−Vps75. All experiments were also performed in the absence of Rtt109−Vps75 to account for thermodynamic changes as a result of ligand dilution.

Gel Filtration Analysis. Gel filtration chromatography was performed on a Superdex 200 10/300GL column from GE and calibrated with Sigma protein standards comprised of albumin from bovine serum, alcohol dehydrogenase from yeast, β-amylase from sweet potato, carbonic anhydrase from bovine erythrocytes, and cytochrome *c* from horse heart. Protein samples (75 μM copurified Rtt109−Vps75 and 50 μM H3−H4) were equilibrated on ice at 4 °C for 60 min in 50 mM Tris (pH 8.0), 215 mM NaCl, and 5% glycerol prior to elution of protein on the column in 50 mM Tris (pH 8.0) and 215 mM NaCl; 100 μL samples were injected onto the columns and eluted at 0.5 mL/min, and 0.5 mL fractions were collected. The presence of protein was monitored by A_{280} and SDS−PAGE analysis.

Rapid-Quench Flow Analysis. Rapid-quench flow experiments were performed on an RQF-64 Rapid Quench Flow Apparatus from Hi-Tech Scientific. In kinetic experiments with saturating substrate concentrations, copurified Rtt109−Vps75 incubated with AcCoA was mixed with H3, quenched with 1% TFA, and analyzed by the filter binding assay. Final reaction conditions consisted of 50 mM Tris (pH 7.5), 1 mM DTT, 200 mM NaCl, 30 μM H3, 30 μM AcCoA, and 1 μM copurified Rtt109−Vps75. The amount of product formed over time best fit to a linear regression curve by least-squares analysis. Single-enzyme turnover experiments were performed under conditions

similar to those described for saturating substrate experiments, with the alteration of 0.4 μM AcCoA in the final assay conditions. The amount of product formed over time best fit to the single-exponential equation (eq 10)

$$[\text{product}] = Ae^{kt} + B \quad (10)$$

where A is the amplitude, k is the first-order rate constant, and B is the total amount of product formed.

pH Analysis of the Rtt109−Vps75-Catalyzed HAT Reaction. Utilizing the filter binding assay under saturating substrate conditions (30 μM AcCoA, 577 μM H3 peptide, 0.2 μM Rtt109, and 0.8 μM Vps75), the k_{cat} was determined from pH 7 to 10. To maintain a constant ionic strength, 50 mM ACES, 25 mM Tris, and 25 mM ethanolamine were utilized. Measurements could not be made below pH 7 or above pH 10 because of protein activity loss at low pH and high background rates caused by the H3 peptide at high pH. We verified that alterations in k_{cat} were not due to protein inactivation or the hydrolysis of AcCoA between pH 7 and 10. Fits for the k_{cat} data were performed using eq 11

$$v = C/(1 + H/K_a) \quad (11)$$

where C is the pH-independent k_{cat} and K_a is the ionization constant of an amino acid residue from either the substrate or the enzyme. To determine whether loss of activity at low pH was due to ionization of groups involved in forming Rtt109−Vps75, similar experiments were performed as described above with the exception of the presence of 5 μM Vps75 in the HAT assay.

Rtt109 D287 and D288 Mutant Studies. Single-point (D287N and D288N) and double-point (D287A/D288A) mutations were made utilizing a Stratagene site-directed mutagenesis kit, and recombinant protein was purified in a manner similar to that of wild-type His-Rtt109. H3 peptide saturation curves were determined in 50 mM Tris (pH 7.5 and 25 °C), 1 mM DTT, 1−2 μM Rtt109 variant, 4 μM Vps75, and 30 μM AcCoA, with the H3 peptide concentration varied from 50 to 500 μM. AcCoA saturation curves were determined in 50 mM Tris (pH 7.5 and 25 °C), 1 mM DTT, 0.1−0.5 μM Rtt109 variant, 4 μM Vps75, and 400 μM H3 peptide, with the AcCoA concentration varied from 0.5 to 30 μM. For pH−rate analysis, reactions were performed in 50 mM ACES, 25 mM Tris, 25 mM ethanolamine (pH 7−9), 1 mM DTT, 3 μM Rtt109 D287A/D288A, 6 μM Vps75, 400 μM H3 peptide, and 60 μM AcCoA.

RESULTS

Measurement of the Binding Affinity between Rtt109 and Vps75. Previous studies demonstrated that histone acetyltransferase Rtt109 and histone chaperone Vps75 can be copurified, resulting in a kinetic complex that is ~100-fold more efficient than Rtt109 alone (*11*). The ability to coexpress and copurify Rtt109 and Vps75 suggested the formation of a tight-binding stable complex. To determine their binding affinity, fluorescence polarization was performed with separately purified Rtt109 and Vps75.

The titration of $Vps75_{dimer}$ (3.2 nM) with Rtt109 (3.7−190 nM) resulted in the formation of Rtt109−Vps75 (Figure 1). The data were fitted to eq 2 and yielded a K_d value of 10 ± 2 nM. Throughout the detailed biochemical and kinetic experiments that follow, Rtt109 and Vps75 were maintained at concentrations that ensured that ≥98% of Rtt109 was bound by Vps75, and thus, the maximally activated complex was enzymatically characterized.

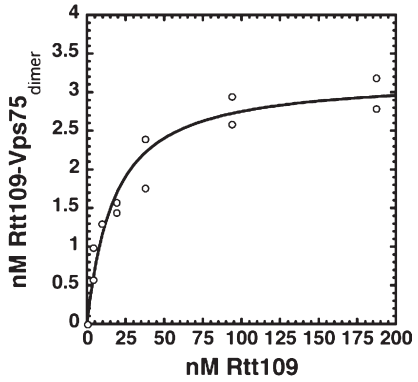

FIGURE 1: Binding of Rtt109 to Vps75. Fluorescein-labeled $Vps75_{dimer}$ (3.2 nM) was titrated with 3.7−190 nM Rtt109 in PBS containing 0.2 mM AcCoA and 0.1 mg/mL BSA at 25 °C and anisotropy measured by fluorescence polarization. Assays were performed seven times in replicate, and a representative figure is shown. Data were fitted to eq 2, yielding a K_d value of 10 ± 2 nM assuming Vps75 exists as a nondissociating dimer.

Steady-State Kinetic Analysis. Rtt109 lacks primary sequence homology with other well-studied HATs, such as GCN5, PCAF, p300, and Esa1 (*25*, *35*−*37*). A striking feature of Rtt109-dependent acetylation is the requirement of a histone chaperone (Asf1 or Vps75) for efficient catalysis (*11*). Therefore, the mechanism of acetylation utilized by Rtt109 is unique, and whether Rtt109 employs similar or distinct catalytic strategies was uncertain. Previously characterized acetyl transfer enzymes bind substrates prior to the direct attack of lysine on the acetyl moiety (sequential mechanism or Theorell−Chance) or form an enzyme−acyl intermediate prior to the transfer of the acyl group onto lysine (ping-pong mechanism) (*35*, *37*, *38*). In the presence of histone chaperone Asf1 or Vps75, Rtt109 displays ~10−100-fold enhancement of histone acetyltransferase activity (*11*, *26*). With Vps75, Rtt109 forms a tight-binding complex that can be copurified, while Asf1 is only loosely associated with Rtt109 (*11*). Here, the detailed kinetic and binding analyses of Rtt109−Vps75 were performed with H3 peptide, H3 protein, or H3−H4 depending on the technical limitations of each assay. Binding order was established with H3−H4, as this is the most physiological substrate; however, it is important to emphasize that the catalytic mechanism is unlikely to be different for the three substrates, especially given the observation that the k_{cat} varies only 5-fold among all three.

To distinguish between a sequential or ping-pong kinetic model, the initial rates of product formation were determined, utilizing the pyruvate dehydrogenase assay as described in Experimental Procedures, at varied concentrations of AcCoA and H3 peptide substrate. To circumvent issues of substrate inhibition and protein precipitation that were observed utilizing high concentrations of full-length H3 protein at low enzyme concentrations and low AcCoA concentrations, the bisubstrate kinetic analysis was performed with H3 peptide (amino acid sequence ARTKQTARKSTGGKAPRKQL), which did not exhibit these effects at high concentrations. The steady-state rates of product formation at varied substrate concentrations were fitted to several kinetic models and plotted in double-reciprocal format for visualization of the resulting patterns. As evident from the plots, a series of intersecting lines patterns consistent with a sequential mechanism were observed at varied concentrations of AcCoA at fixed, varied concentrations of H3 peptide, and vice versa (Figure 2A,B). Furthermore, the clear

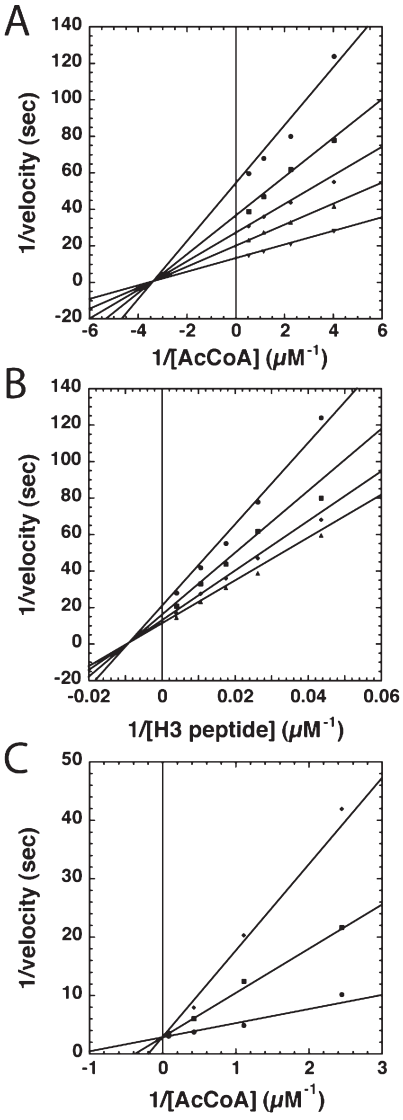

FIGURE 2: Bisubstrate kinetic analysis and CoA product inhibition of Rtt109−Vps75. Experiments were performed two or three times with a representative figure shown. The average of a representative duplicate data set is displayed in double-reciprocal format. Bisubstrate reaction mixtures (A and B) contained 25 mM Tris (pH 7.5 and 25 °C), 1 mM DTT, 0.1 μM Rtt109, and 0.8 μM Vps75. Initial rates were monitored by the pyruvate dehydrogenase assay and data were fitted to eq 3 (see Table 1 for kinetic constants). CoA product inhibition reaction mixtures (C) contained 50 mM Tris (pH 7.5 and 25 °C), 1 mM DTT, 20 nM Rtt109, and 0.8 μM Vps75 utilizing the filter binding assay and data were fitted to eq 6, yielding a K_{is} value of 110 ± 20. (A) Varied AcCoA concentrations at fixed and varied H3 peptide concentrations: 23 (●), 38 (■), 58 (◆), 96 (▲), and 262 μM H3 peptide (▼). (B) Varied H3 peptide concentrations at fixed and varied AcCoA concentrations: 0.25 (●), 0.45 (■), 0.9 (◆), and 2 μM AcCoA (▲). (C) Varied AcCoA concentrations at a fixed CoA concentration (5 μM): 0 (●), 250 (■), and 600 μM H3 (◆).

absence of a parallel line pattern as determined by visual inspection and statistical analysis suggests Rtt109 does not utilize a ping-pong mechanism. The data were fitted to a sequential kinetic model (eq 3) and yielded the following kinetic constants: $K_m = 0.3 \pm 0.1$ μM and $k_{cat}/K_m = (3.9 \pm 0.5) \times 10^5$ M^{-1} s^{-1} for AcCoA, and $K_m = 112 \pm 11$ μM and $k_{cat}/K_m = (9.8 \pm 0.9) \times 10^2$ M^{-1} s^{-1} for the H3 peptide (Table 1). The k_{cat} value of Rtt109-Vps75 (0.11 ± 0.01 s^{-1}) toward H3 peptide substrate is approximately 5-fold lower than that of Rtt109−Vps75 toward full-length H3 substrate (0.62 ± 0.03 s^{-1}) (Table 1). Together, these data provide evidence of a sequential mechanism in which both substrates must be bound in the active site before chemical catalysis.

CoA Product Inhibition of Rtt109−Vps75. To establish the order of substrate binding and product release, inhibition studies were performed using CoA as a product inhibitor. Here, we varied the AcCoA concentration at several fixed concentrations of CoA and a fixed full-length H3 concentration (5 μM) and plotted the rate data in double-reciprocal format. The resulting line pattern intersects at the *y*-axis, which is diagnostic of competitive inhibition. A parallel line pattern and an intersecting line pattern in the second or third quadrants would have demonstrated uncompetitive and noncompetitive inhibition, respectively (Figure 2C). Fitting the data to the equation for competitive inhibition (eq 6) yielded a K_{is} value of 110 ± 20 μM for CoA. The lack of a *y*-intercept effect ($1/v$) indicates that AcCoA and CoA both compete for the same enzyme form. This result supports a mechanism in which Rtt109−Vps75 can bind to AcCoA prior to H3 but does not exclude random binding of substrates. Because Rtt109−Vps75 can acetylate multiple residues on the tail and globular fold of H3, it was not technically feasible to generate a fully acetylated H3 peptide sufficiently soluble to perform product inhibition analysis (*26*). Creating an acetylated H3 full-length product inhibitor was also not a viable option, as Rtt109−Vps75 is able to acetylate numerous lysines, albeit at slower rates. Next, we sought to directly measure binding affinities of AcCoA and CoA for Rtt109−Vps75.

AcCoA and CoA Binding to Rtt109−Vps75. To provide direct evidence of AcCoA and CoA binding to free Rtt109−Vps75, isothermal titration calorimetry (ITC) was utilized. In each experiment, AcCoA or CoA was titrated into Rtt109−Vps75 and heats of binding were measured (Figure 3A,B). The binding isotherms revealed saturable binding consistent with a one-site model in which AcCoA bound to Rtt109−Vps75 with a K_d value of 1.4 ± 0.3 μM, while CoA yielded a K_d value of 43 ± 5 μM (Figure 3 and Table 1 of the Supporting Information). These values are in good agreement with the dissociation constants determined from fluorescence measurements (*22*). Additionally, the K_d value for CoA is similar to the inhibition constant obtained for CoA ($K_{is} = 110 \pm 20$ μM). The decreased binding affinity of CoA for Rtt109−Vps75 compared to that of AcCoA reveals the contribution of the acetyl group to overall binding.

Binding of CoA to Rtt109−Vps75 in the Presence of H3 Substrate. If H3 bound first and promoted binding of AcCoA to Rtt109−Vps75, one would predict an increase in affinity for AcCoA in the presence of an H3 substrate. Because the presence of AcCoA and H3 substrate would result in product turnover by Rtt109−Vps75 and interfere with equilibrium binding measurements, we performed ITC by titrating CoA into Rtt109−Vps75 in the presence of saturating concentrations of H3 peptide (577 μM), leading to the formation of a dead-end substrate−product complex. The presence of the H3 peptide did not enhance the binding of CoA to Rtt109−Vps75 (K_d of 44 ± 3 μM compared to a value of 43 ± 5 μM without peptide) (Table 2 and Figure 1 of the Supporting Information). Together, the product inhibition and binding studies provide support for a kinetic mechanism in which AcCoA can bind prior to H3 substrate, and the presence of H3 peptide does not alter the binding affinity of AcCoA. It should be noted that H3 peptide yields a K_m value that is 2 orders of magnitude higher than that for full-length H3 and 3 orders of a magnitude higher than that observed with AcCoA. Therefore,

Table 1: Summary of Steady-State Kinetic Constants for Rtt109−Vps75[a]

Rtt109 enzyme	substrate (s^{-1})	k_{cat} (s^{-1})	K_m (μM)	k_{cat}/K_m (M^{-1} s^{-1})
wild type	AcCoA	0.11 ± 0.01	0.3 ± 0.1	$(3.9 \pm 0.5) \times 10^5$
	H3 peptide	0.11 ± 0.01	112 ± 11	$(9.8 \pm 0.9) \times 10^2$
	full-length H3[b]	0.62 ± 0.03	7 ± 1	$(9 \pm 1) \times 10^4$
D287N	AcCoA	$(1.2 \pm 0.1) \times 10^{-2}$	0.7 ± 0.3	$(1.7 \pm 0.7) \times 10^4$
	H3 peptide	$(8.7 \pm 0.4) \times 10^{-3}$	62 ± 8	$(1.4 \pm 0.2) \times 10^2$
D288N	AcCoA	$(2.8 \pm 0.2) \times 10^{-3}$	4.9 ± 0.9	$(6 \pm 1) \times 10^2$
	H3 peptide	$(2.1 \pm 0.1) \times 10^{-3}$	55 ± 11	$(3.8 \pm 0.8) \times 10$
D287A/D288A	H3 peptide	$(1.1 \pm 0.1) \times 10^{-3}$	44 ± 7	$(2.5 \pm 0.4) \times 10$

[a]Standard errors are reported. All assays were performed in the presence of H3 peptide with the exception of the case in which full-length H3 was utilized as indicated. [b]Full-length H3 saturation curve determined in 50 mM Tris, 1 mM DTT, 0.2 μM Rtt109, 1.6 μM Vps75, 50 AcCoA, and 2−32 μM full-length H3.

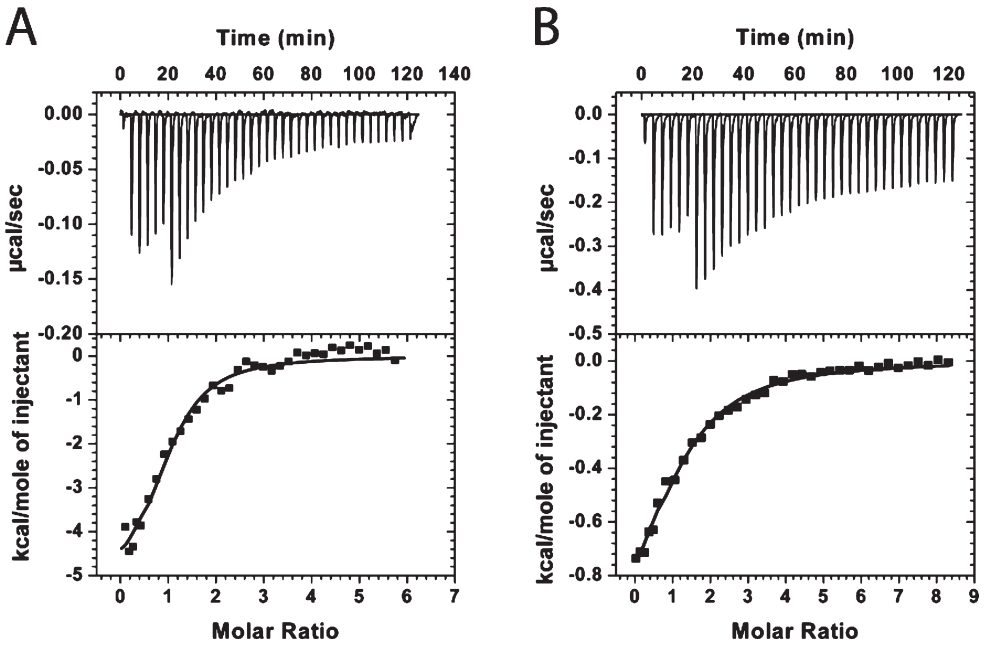

FIGURE 3: ITC profile of Rtt109−Vps75 with AcCoA and CoA. (A) AcCoA was titrated into Rtt109−Vps75. The top graph shows data obtained for 37 automatic injections (1−8 μL) of AcCoA into copurified Rtt109−Vps75. The bottom graph shows the integrated curve showing experimental points (■) fitted to a one-site binding curve (—). AcCoA (167 μM) was injected into 5.8 μM Rtt109−Vps75, yielding a K_d value of 1.4 ± 0.3 μM. Buffer conditions: 50 mM Tris (pH 7.5 and 25 °C), 5% (w/v) glycerol, 50 mM NaCl, 2 mM β-mercaptoethanol, and 1 mM EDTA. (B) CoA was titrated into Rtt109−Vps75, yielding a K_d value of 43 ± 5 μM. CoA (2 mM) was injected into 50 μM copurified Rtt109−Vps75. Buffer conditions are the same as those for panel A.

when H3 peptide is the substrate, AcCoA binding may precede H3 peptide binding.

Analysis of H3 Substrates Binding to Rtt109−Vps75. Given that Rtt109 forms a tight complex with Vps75 and that the histone chaperone is capable of binding H3, we determined whether Rtt109−Vps75 is able to bind H3 in the absence of AcCoA. First, H3 peptide was titrated into Rtt109−Vps75, and heats of binding were monitored by ITC (Figure 2 of the Supporting Information). These binding measurements yielded a K_d value of 103 ± 7 μM, which is in agreement with the K_m value of 112 ± 11 μM for H3 peptide (Table 1 of the Supporting Information and Table 1). We were unable to perform direct binding studies for binding of the H3 protein to Rtt109−Vps75 because protein precipitation occurred at concentrations necessary for ITC measurements. To provide further support for the ability of H3 substrate to bind Rtt109−Vps75 prior to AcCoA binding, we performed a binding analysis utilizing gel filtration, a technique that allows for the resolution of protein complexes on the basis of relative size and shape. Preparations of Rtt109−Vsp75 alone, H3−H4 alone, and a mixture containing Rtt109−Vps75 (in stoichiometric excess) with H3−H4 were resolved on a gel filtration column (Superdex 200 10/300 GL from GE). We attempted to analyze full-length H3 and Rtt109−Vps75 mixtures but were unable to combine these proteins in sufficient quantities without protein precipitation. As shown by SDS−PAGE analysis of fractions eluted from the gel filtration column, Rtt109−Vps75 eluted at ~13 mL and H3−H4 eluted at ~15 mL (Figure 4). Preparations of H3−H4 and Rtt109−Vps75 coelute at ~11 mL, as expected for the formation of a complex larger than either H3−H4 or Rtt109−Vps75 alone (Figure 4). Because Rtt109−Vps75 is able to form a stable complex with H3 substrates in the absence of AcCoA, substrate binding is likely random, or at the very least not strictly ordered.

Rapid-Quench Kinetics. Rapid-quench kinetic analysis was used to determine whether substrate binding, chemical catalysis, or product release is the rate-limiting step. This rapid kinetic approach permits millisecond quenching of the reaction and allows one to measure the rate of product formation during the first enzyme turnover. If a burst of product (acetylated H3) is

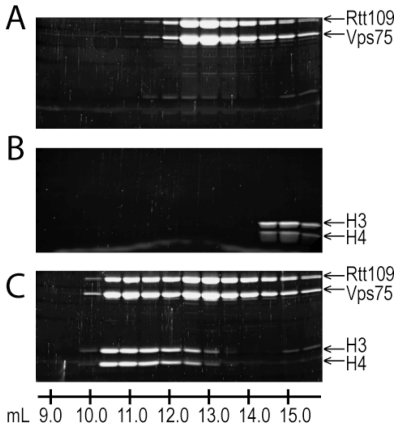

FIGURE 4: Gel filtration analysis of Rtt109−Vps75 and H3−H4. Shown are elution profiles of protein complexes from gel filtration chromatography. Samples from elution fractions were analyzed by SDS−PAGE followed by Ruby-Sypro staining of 12% SDS−PAGE gels. The data below the gel (mL) are approximate volumes of protein elution from column chromatography. (A) SDS−PAGE gel of copurified Rtt109−Vps75 (75 μM). (B) SDS−PAGE gel of H3−H4 (50 μM). (C) SDS−PAGE gel for a mixed sample of copurified Rtt109−Vps75 (75 μM) and H3−H4 (50 μM).

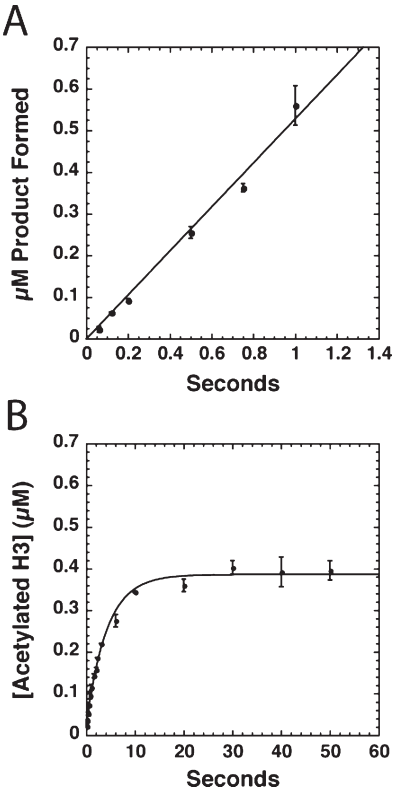

FIGURE 5: Rapid quench kinetics of Rtt109−Vps75. (A) Reactions were performed in 50 mM Tris-HCl (pH 7.5), 200 mM NaCl, and 1 mM DTT. Using a Hi-Tech quench flow device, copurified Rtt109−Vps75 (1 μM) and AcCoA (30 μM) were rapidly mixed with H3 (30 μM) (concentrations after mixing). Reactions were quenched with 1% TFA after 60 ms to 10 s. Data were fitted to a linear regression equation to determine the turnover rate. Error bars represent the standard deviation. Experiments were performed twice in duplicate, yielding a rate of 0.53 ± 0.02 s^{-1}. (B) Reaction conditions were similar to multiple-turnover RQF experiments with AcCoA (0.4 μM) limiting enzyme turnover. Reactions were quenched from 120 ms to 50 s. Experiments were performed twice in duplicate and data were fitted to eq 10, yielding a rate of 0.59 ± 0.05 s^{-1}.

formed followed by a slower steady-state rate of product formation, then product release is likely rate-limiting in turnover. Alternatively, the presence of a lag phase early in the reaction can be indicative of substrate binding (i.e., substrate-induced conformational change) as rate-limiting. Lastly, linear product formation is suggestive of chemical catalysis as a slow step in the kinetic cycle. To distinguish the kinetic behavior for Rtt109−Vps75 during the early phase of the reaction (millisecond range), we measured the amount of product formed with excess (multiple-turnover) concentrations of AcCoA and H3 protein substrate. Specifically, Rtt109−Vps75, preincubated with AcCoA, was rapidly reacted with H3 substrate, and the reaction was quenched with 1% TFA at varied times between 60 ms and 1 s. The amount of acetylated product was then quantified via a filter binding HAT assay. The amount of product formed over time produced a linear curve yielding a rate of 0.53 ± 0.02 s^{-1}, which is in good agreement with the steady-state k_{cat} value of 0.62 ± 0.03 s^{-1} (Figure 5A and Table 1). A burst or lag was undetectable, providing compelling evidence that the chemical step of the transfer of an acetyl group from AcCoA to H3 is the rate-limiting step (Figure 5A).

To provide additional support for rate-limiting acetyl transfer, single-turnover experiments in which substoichiometric amounts of AcCoA were preincubated with Rtt109−Vps75 and reacted with saturating amounts of H3 protein were performed (final concentrations of 1 μM Rtt109−Vps75, 0.4 μM AcCoA, and 30 μM H3). The amount of acetylated product formed over time was fitted to a first-order exponential equation (eq 10) where $k = 0.59 \pm 0.05$ s^{-1}, which is in excellent agreement with the value of 0.53 ± 0.02 s^{-1} determined from the rapid-quench experiments under multiple-turnover conditions (Figure 5B). Together, these data indicate that chemical catalysis is rate-limiting for the overall Rtt109−Vps75-catalyzed reaction.

pH Profile Analysis. To identify ionizations that are critical for catalysis, a k_{cat}−pH profile analysis of Rtt109 (0.2 μM) with Vsp75 (0.8 μM) was performed. To monitor the pH dependence of k_{cat}, initial rates of product formation were measured under saturating concentrations of AcCoA and H3 peptide and at varied pHs (7−10). The observed rates increased with an increase in pH until a plateau of activity was reached above pH 8.5 (Figure 6A). The data were fitted to a curve that described a single critical ionization that must be unprotonated for activity (eq 11), yielding a pK_a value of 8.5 ± 0.1 and a pH-independent k_{cat} value of 0.53 ± 0.05 s^{-1}. To verify that the ionization with a pK_a of 8.5 was not due to an ionizable residue that caused dissociation of Rtt109 and Vps75 at low pH, the ability of increased levels of Vps75 to activate Rtt109 (0.2 μM) was evaluated at pH 7 and 8. The addition of a 6.25-fold excess of Vps75 (5 μM compared to 0.8 μM) did not increase initial rates of product formation at pH 7 or 8 (Figure 6B). The lack of rescue of Rtt109−Vps75 activity by addition of additional Vps75 suggests the critical ionization observed in the pH profile is not due to an ionizable group that affects association of Rtt109−Vps75. Thus, the pH−rate analysis indicates a group with a pK_a of 8.5 must be unprotonated for catalysis.

Analysis of Rtt109 D287 and D288 Variants. Previously, kinetic analysis of several HATs such as GCN5, PCAF, and Esa1 indicated the involvement of a general base (glutamate or aspartate) that facilitates the deprotonation of the ε-amino group of the lysine substrate, which is required for the nucleophilic attack of bound AcCoA (*35*, *36*, *39*). In Esa1, mutation of the general base catalyst Glu338 (E338Q) resulted in an upward shift of the pK_a (1.4 pH units) of an ionizable group (*35*). Although the

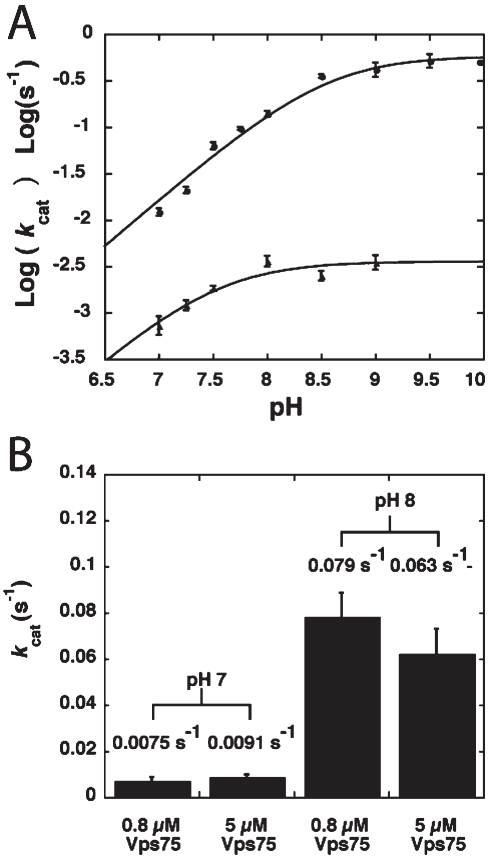

FIGURE 6: k_{cat}−pH analysis of wild-type and D287A/D288A Rtt109−Vps75. (A) Profiles of the pH dependence of k_{cat}. Reaction mixtures contained 50 mM ACES, 25 mM Tris, and 25 mM ethanolamine buffer (ATE buffer) at 25 °C, 1 mM DTT, and saturating AcCoA and H3 peptide concentrations. Initial rates of product formation were measured by a filter binding HAT assay. Experiments were performed twice in duplicate and data were fitted to eq 11. For the wild-type enzyme (●), 0.2 μM Rtt109 and 0.8 μM Vps75 were utilized, yielding a pK_a of 8.5 ± 0.1. For experiments with D287A/D288A Rtt109 (▲), 2 μM D287A/D288A Rtt109 and 4 μM Vps75 were utilized, yielding a pK_a of 7.5 ± 0.1. (B) Conditions similar to those used for panel A. Vps75 (0.8 or 5 μM) was added to Rtt109 (0.2 μM) at pH 7 or 8 to determine whether increasing the Vps75 concentration increases the rate of acetylation of the H3 peptide by Rtt109. Experiments were performed three times in duplicate, with error bars representing the standard deviation.

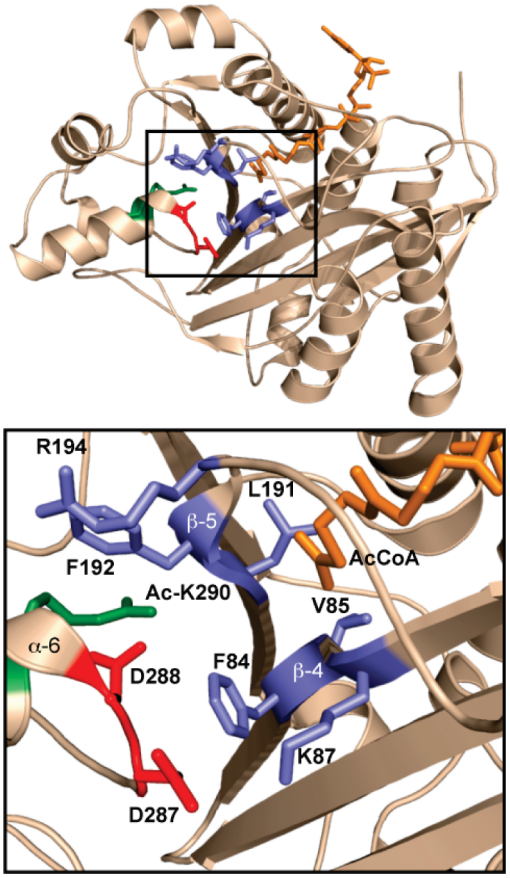

FIGURE 7: Putative lysine binding site of Rtt109 bound to AcCoA. Ribbon model of the Rtt109 overall structure and zoomed-in view of the active site (Protein Data Bank entry 3D35). AcCoA (orange), residues of the hydrophobic pocket (blue), D287 (red), D288 (red), and K290 (green) are shown as stick models. α-Helix 6, β-sheet 4, and β sheet 5 are denoted.

E338Q enzyme displayed severe catalytic impairment at neutral and low pH values, at pH >9, the E338Q variant is nearly as efficient as the wild-type enzyme. We concluded that E338 acts to facilitate the removal of a proton from lysine, and this function is dispensable at high pH values where the ε-amino group is largely unprotonated. The crystal structure of Rtt109(Δ130−179) did not reveal obvious ionizable groups in the proximity of the acetyl group of bound AcCoA (*22*). However, D287 and D288 are conserved amino acid residues that reside in the active site, ~8−11 Å from AcCoA, and could potentially have roles in catalysis (Figure 7) (*22*).

To dissect the importance of these residues, we generated single-glutamine variants (D288N and D288N) and a double-alanine variant of Rtt109 (D287A/D288A), and steady-state kinetic analyses were performed in the presence of Vps75. H3 peptide saturation curves showed an ~50-fold loss of activity for the D288N Rtt109 variant [k_{cat} = (2.1 ± 0.1) × 10^{-3} s^{-1}] compared to wild-type enzyme [k_{cat} = (1.1 ± 0.1) × 10^{-1} s^{-1}] (Table 1). The D287N variant [k_{cat} = (8.7 ± 0.4) × 10^{-3} s^{-1}] was less affected, with an ~10-fold decrease in activity (Table 1). Minimal alteration was noted for the peptide K_m values for these variants [K_m of 62 ± 8 μM for Rtt109 D287N and 55 ± 11 μM for Rtt109 D288N compared to a K_m of 112 ± 11 μM for wild-type Rtt109 (Table 1)]. An ~16-fold increase in K_m for AcCoA was observed for the D288N mutant (K_m = 4.9 ± 0.9 μM) compared to the wild-type enzyme (K_m = 0.3 ± 0.1 μM), and strikingly, the k_{cat}/K_m decreased by ~3 orders of magnitude [k_{cat}/K_m of (3.9 ± 0.5) × 10^5 M^{-1} s^{-1} for the wild type vs a value of (6 ± 1) × 10^{-2} M^{-1} s^{-1} for D288N]. Little change in K_m with AcCoA was observed for D287N (K_m = 0.7 ± 0.3 μM). To investigate if the remaining aspartic acid could compensate for the mutated residue in the single-amino acid variants, a double mutant (D287A/D288A) was analyzed. The D287A/D288A variant yielded an ~100-fold k_{cat} decrease [k_{cat} = (1.1 ± 0.1) × 10^{-3} s^{-1}] compared to the wild-type enzyme. Taken together, these results argue against the ability for D287 or D288 to compensate in catalysis (Table 1). Moreover, the D288 substitution appears to account for most of the activity loss of the D287A/D288A variant (Table 1). Similar to the single-site variants, the D287A/D288A variant displayed a minimal change in the K_m for the H3 peptide [K_m = 44 ± 7 μM (Table 1)]. To determine if D287 or D288 in Rtt109−Vps75 acts as a base catalyst, we monitored the pH dependence of k_{cat} with the D287A/D288A variant, revealing a slight decrease in the pK_a (7.5 ± 0.1) compared to that of the wild-type complex (Figure 6A). This is in contrast to other HAT enzymes that utilize general base catalysis and display an increase in the pK_a of an ionizable group with mutation of the general base.

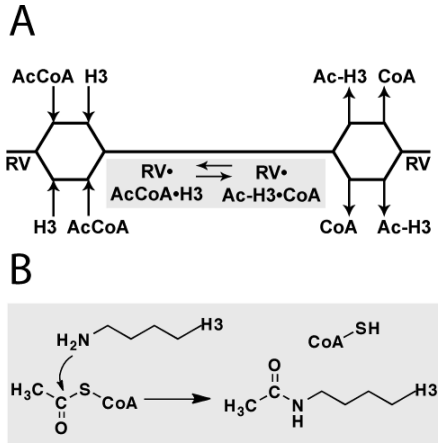

FIGURE 8: Proposed kinetic mechanism of acetylation of H3 substrate by Rtt109−Vps75. (a) Cleland diagram of the kinetic mechanism. RV is Rtt109−Vps75. H3 is the H3 substrate. (B) Chemistry of catalysis. The lysine of H3 attacks AcCoA with acetyl transfer following.

These data argue against a role for D287 or D288 in general base catalysis.

DISCUSSION

Rtt109 is a novel HAT (KAT) that lacks sequence similarity to other well-characterized CoA-dependent acetyltransferases and requires association with a histone chaperone for efficient catalysis. In this study, we sought to understand the catalytic mechanism for this unique high-affinity histone chaperone−HAT complex and performed detailed kinetic and binding analyses that support a random sequential (direct attack) mechanism (Figure 8). We propose that AcCoA and H3 (or H3−H4) bind to Rtt109−Vps75 without obligate order, forming a ternary complex (enzyme·AcCoA·H3), whereby the ε-amino group of lysine directly attacks the acetyl group of bound AcCoA (Figure 8). After the transfer of the acetyl group to the substrate lysine, acetylated H3 and CoA are released in either ordered or random fashion (Figure 8). Using rapid-quench techniques, we provided evidence consistent with chemical catalysis being the rate-limiting step in turnover. From pH−rate analyses, we propose that the ionizable group that must be unprotonated for catalysis reflects the lysine ε-amine of the bound substrate.

Several lines of evidence support the conclusion that Vps75 and Rtt109 form a reversible, high-affinity interaction that represents the catalytically maximized complex. First, direct binding measurements yielded nanomolar K_d values (~10 nM) of the complex. Furthermore, similar k_{cat} values were attained whether micromolar (i.e., RQF) or submicromolar protein concentrations were utilized (i.e., steady-state analysis), consistent with low nanomolar K_d values and a Rtt109−Vps75 that was maximally activated. We also observed that co-expression of Rtt109−Vps75, followed by resolution over nickel affinity, anion exchange, and gel filtration, maintained the complex and that only a strong hydrophobic interaction column (Phenyl Sepharose) could disrupt their interaction. After Rtt109 and Vps75 had been separated by hydrophobic interaction chromatography, recombining the two proteins produced a fully activated complex, demonstrating the reversibility of binding. Consistent with a high-affinity complex, endogenous Rtt109 copurifies with Vps75 in yeast (*5*, *27*, *40*, *41*). Previously, two other laboratories reported a lower-affinity interaction between Vps75 and Rtt109 (K_d = 2.7 to ~5 μM) (*20*, *42*). While it is unclear what this low-affinity interaction represents, here, we observed no significant changes in catalytic efficiency at higher protein concentrations (~1 μM), suggesting that this binding event does not markedly alter catalysis. Alternatively, this discrepancy may be the result of different methods, protein constructs, or binding conditions used by others. For example, we find that Rtt109 alone is an unstable protein and is highly prone to aggregation, and inclusion of AcCoA during the binding assays stabilized Rtt109 and prevented aggregation.

Unlike other HAT enzymes that require obligate-ordered substrate binding (AcCoA followed by histone substrates) (*25*, *36*, *37*), a unique feature of Rtt109−Vps75 is the random binding of substrates (Figure 8). In such a mechanism, it is predicted that one substrate should be able to bind in a manner independent of the other, and the binding of substrate will not significantly enhance the binding of the second. From product inhibition studies, CoA exhibited competitive inhibition against AcCoA, indicating AcCoA and CoA can bind to the same enzyme form, yielding an Rtt109−Vps75·AcCoA or Rtt109−Vps75·CoA complex (Figure 8). Equilibrium binding studies revealed both AcCoA and CoA bind to Rtt109−Vps75, and no increase in binding affinity is observed when CoA binding is assessed in the presence of the H3 peptide. Additionally, H3−H4 formed a tight-binding complex with Rtt109−Vps75 in the absence of AcCoA, as demonstrated by gel filtration analysis. Also consistent with a random substrate binding model, the H3 peptide is able to bind Rtt109−Vps75 in the absence of AcCoA. Interestingly, p300, the likely mammalian structural ortholog of Rtt109, requires binding of AcCoA prior to binding histone substrates, revealing that although Rtt109 and p300 share roles in acetylating lysine 56 of H3, their kinetic mechanisms differ (*25*, *43*). Other key differences between Rtt109 and p300 are highlighted by the fact that p300 has efficient HAT activity in the absence of histone chaperones and likely displays wider substrate specificity, including both histone and non-histone substrates (*43*, *44*).

The pre-steady-state kinetic analysis provides strong support for acetyl group transfer as the rate-limiting step in catalysis at pH 7.5. The observed rates in both multiple- and single-turnover experiments are in agreement with the steady-state k_{cat} value. The lack of a discernible lag or burst phase during multiple-turnover conditions argues against substrate binding or product release as the rate-limiting step in catalysis. Given that the k_{cat} reflects the chemical step of catalysis, the effect of pH on the k_{cat} reveals information about how chemical catalysis is accomplished by Rtt109−Vps75.

The pH−k_{cat} analysis of Rtt109−Vps75 revealed an ionizable group (pK_a = 8.5) that must be unprotonated for efficient catalysis. Because of the proximity of two conserved aspartic acid residues (D287 and D288) near the putative active site, we investigated whether these residues have a role in deprotonating the ε-amino group of lysine (Figure 7) (*22*−*24*). The mutational analysis revealed there were substantial effects on catalysis, which were reflected by the large ~50−100-fold decrease in the k_{cat} of the D288N and D287A/D288A variants. However, pH−k_{cat} analysis of D287A/D288A did not eliminate or cause an upward shift in the pK_a value as we would expect for the loss of a general base catalyst and the unassisted deprotonation of the lysine. In fact, the apparent pK_a value for the D287A/D288A mutant was shifted downward by ~1 pH unit. These results are in contrast to other previously characterized HATs that utilize a general base

mechanism, where the pK_a value of ~8 represents the hydrogen-bonded ion pair between the N-ε-lysine and the general base glutamate or aspartate (*35*, *36*, *39*).

Because neither D287 nor D288 is not likely responsible for the ionization in the k_{cat}−pH profiles, we propose that the pH-dependent ionization reflects the enzyme-bound lysine of H3 substrate, which is perturbed when bound in the hydrophobic active site. The crystal structures of Rtt109 reveal a hydrophobic active site that creates an environment favoring the neutralized, unprotonated state of the substrate lysine (Figure 7). Residues that line the hydrophobic "tunnel" include F84, V85, and the aliphatic side chain of K87 on β-sheet 4, as well as L191, F192, and the aliphatic side chain of R194 on β-sheet 5 of Rtt109 (Figure 7). Rtt109 may increase the nucleophilicity of the substrate lysine by perturbing the pK_a of lysine downward to ~8.5 within the hydrophobic tunnel of the enzyme·AcCoA·H3 complex. Perturbation of the pK_a values of ionizable groups arises from the energetically unfavorable process of transferring a charged group from a high-dielectric constant environment (i.e., water) to a less polar environment, such as the burial of the charged group in the interior of a protein environment. For example, a V66K mutant in staphylococcal nuclease displayed a pK_a value of 10.2 in the denatured state compared to the pK_a value of 6.4 in the native state (*45*, *46*). This downward shift in pK_a is suggested to favor the uncharged form of lysine 66 within the context of the hydrophobic interior of the folded protein. Interestingly, p300, the closest structural homologue of Rtt109 in mammals, also appears to lack a putative general base (*25*). Like that by Rtt109, catalysis by p300 revealed the requirement of an ionizable group (pK_a = 8.4), and the X-ray structure revealed a very hydrophobic active site (*25*).

Our steady-state analysis revealed a critical role for aspartate 288 of Rtt109, as mutation resulted in both k_{cat}/K_m and k_{cat} defects. An ~16-fold increase in K_m for AcCoA and an ~50-fold decrease in k_{cat} were observed for the D288N mutant compared to wild-type enzyme. Thus, the k_{cat}/K_m for AcCoA was decreased by ~3 orders of magnitude. This large k_{cat}/K_m effect may reflect a role for D288 in AcCoA binding. Surprisingly, D288 of Rtt109 lies ~8 Å from AcCoA in the active site, suggesting that direct interaction between AcCoA and D288 is unlikely (*22*−*24*).

One potential role for D288 may be linked to its interaction with acetylated K290 of Rtt109. As shown by mass spectrometric analysis, previous studies demonstrated that K290 is nearly completely acetylated in both affinity-purified TAP-tagged Rtt109 from yeast and Rtt109 [Rtt109(Δ130−179)] expressed in bacteria (Figure 7) (*22*). Three independently determined crystal structures of Rtt109 revealed electron density at lysine 290 consistent with an acetyl group, while genetic analysis indicated that mutation of this residue produced defective Rtt109 in vivo (*22*−*24*). Additionally, wild-type Rtt109 used in our analyses is fully acetylated at K290, while the D287A/D288A mutant is mostly unacetylated at K290 (B. N. Albaugh and J. M. Denu, unpublished data). Together, these studies suggest a role for D288 in autoacetylation. The structures of Rtt109 show D288 and K290 residing on α-helix 6, forming a "lid" domain that interacts with the hydrophobic core domain of Rtt109, including β-sheet 5 which partially houses the acetyl group of AcCoA (Figure 7) (*22*−*24*). The interaction of α-helix 6 with the core domain results in the burial of acetylated K290 within the hydrophobic core and formation of a hydrogen bond interaction between D288 and acetylated K290 (*22*−*24*). D288 might properly position acetylated K290 or facilitate the chemistry of autoacetylation (i.e., general base), whereupon mutation of this residue prevents K290 acetylation. An unfavorable interaction of positively charged K290 with the core interior could perturb a local rearrangement of the acetyl binding pocket of AcCoA, as reflected by the large k_{cat}/K_m defect. Interestingly, Rtt109−Vps75 displays a 30-fold higher binding affinity for AcCoA over CoA, indicating that the acetyl group significantly contributes to overall AcCoA binding, and this acetyl-specific interaction might be disrupted in the D288N Rtt109 mutant. A multifaceted layer of regulation for Rtt109 exists, governed by interactions with histone chaperones and autoacetylation of K290. Current efforts are directed at providing a detailed understanding of the functional role of K290 autoacetylation and the involvement of D288 in this modification, as well as the potentially distinct mechanisms of activation mediated by histone chaperones Asf1 and Vps75.

ACKNOWLEDGMENT

We thank all members in the lab of John Denu for helpful discussions.

SUPPORTING INFORMATION AVAILABLE

Additional experimental details, thermodynamic table, and isothermal titration calorimetry results. This material is available free of charge via the Internet at http://pubs.acs.org.

REFERENCES

1. Latham, J. A., and Dent, S. Y. (2007) Cross-regulation of histone modifications. *Nat. Struct. Mol. Biol. 14*, 1017–1024.
2. Bhaumik, S. R., Smith, E., and Shilatifard, A. (2007) Covalent modifications of histones during development and disease pathogenesis. *Nat. Struct. Mol. Biol. 14*, 1008–1016.
3. Ozdemir, A., Masumoto, H., Fitzjohn, P., Verreault, A., and Logie, C. (2006) Histone H3 lysine 56 acetylation: A new twist in the chromosome cycle. *Cell Cycle 5*, 2602–2608.
4. Xhemalce, B., Miller, K. M., Driscoll, R., Masumoto, H., Jackson, S. P., Kouzarides, T., Verreault, A., and Arcangioli, B. (2007) Regulation of histone H3 lysine 56 acetylation in *Schizosaccharomyces pombe*. *J. Biol. Chem. 282*, 15040–15047.
5. Han, J., Zhou, H., Horazdovsky, B., Zhang, K., Xu, R. M., and Zhang, Z. (2007) Rtt109 acetylates histone H3 lysine 56 and functions in DNA replication. *Science 315*, 653–655.
6. Driscoll, R., Hudson, A., and Jackson, S. P. (2007) Yeast Rtt109 promotes genome stability by acetylating histone H3 on lysine 56. *Science 315*, 649–652.
7. Celic, I., Masumoto, H., Griffith, W. P., Meluh, P., Cotter, R. J., Boeke, J. D., and Verreault, A. (2006) The sirtuins hst3 and Hst4p preserve genome integrity by controlling histone h3 lysine 56 deacetylation. *Curr. Biol. 16*, 1280–1289.
8. Maas, N. L., Miller, K. M., DeFazio, L. G., and Toczyski, D. P. (2006) Cell cycle and checkpoint regulation of histone H3 K56 acetylation by Hst3 and Hst4. *Mol. Cell 23*, 109–119.
9. Masumoto, H., Hawke, D., Kobayashi, R., and Verreault, A. (2005) A role for cell-cycle-regulated histone H3 lysine 56 acetylation in the DNA damage response. *Nature 436*, 294–298.
10. Chen, C. C., Carson, J. J., Feser, J., Tamburini, B., Zabaronick, S., Linger, J., and Tyler, J. K. (2008) Acetylated lysine 56 on histone H3 drives chromatin assembly after repair and signals for the completion of repair. *Cell 134*, 231–243.
11. Tsubota, T., Berndsen, C. E., Erkmann, J. A., Smith, C. L., Yang, L., Freitas, M. A., Denu, J. M., and Kaufman, P. D. (2007) Histone H3-K56 acetylation is catalyzed by histone chaperone-dependent complexes. *Mol. Cell 25*, 703–712.
12. Williams, S. K., Truong, D., and Tyler, J. K. (2008) Acetylation in the globular core of histone H3 on lysine-56 promotes chromatin disassembly during transcriptional activation. *Proc. Natl. Acad. Sci. U.S.A. 105*, 9000–9005.
13. Xu, F., Zhang, Q., Zhang, K., Xie, W., and Grunstein, M. (2007) Sir2 deacetylates histone H3 lysine 56 to regulate telomeric heterochromatin structure in yeast. *Mol. Cell 27*, 890–900.

14. Yuan, J., Pu, M., Zhang, Z., and Lou, Z. (2009) Histone H3-K56 acetylation is important for genomic stability in mammals. *Cell Cycle 8*, 1747–1753.
15. Xie, W., Song, C., Young, N. L., Sperling, A. S., Xu, F., Sridharan, R., Conway, A. E., Garcia, B. A., Plath, K., Clark, A. T., and Grunstein, M. (2009) Histone h3 lysine 56 acetylation is linked to the core transcriptional network in human embryonic stem cells. *Mol. Cell 33*, 417–427.
16. Park, Y. J., and Luger, K. (2008) Histone chaperones in nucleosome eviction and histone exchange. *Curr. Opin. Struct. Biol. 18*, 282–289.
17. Li, Q., Zhou, H., Wurtele, H., Davies, B., Horazdovsky, B., Verreault, A., and Zhang, Z. (2008) Acetylation of histone H3 lysine 56 regulates replication-coupled nucleosome assembly. *Cell 134*, 244–255.
18. Selth, L. A., Lorch, Y., Ocampo-Hafalla, M. T., Mitter, R., Shales, M., Krogan, N. J., Kornberg, R. D., and Svejstrup, J. Q. (2009) An rtt109-independent role for vps75 in transcription-associated nucleosome dynamics. *Mol. Cell. Biol. 29*, 4220–4234.
19. Selth, L., and Svejstrup, J. Q. (2007) Vps75, a new yeast member of the NAP histone chaperone family. *J. Biol. Chem. 282*, 12358–12362.
20. Park, Y. J., Sudhoff, K. B., Andrews, A. J., Stargell, L. A., and Luger, K. (2008) Histone chaperone specificity in Rtt109 activation. *Nat. Struct. Mol. Biol. 15*, 957–964.
21. Allis, C. D., Berger, S. L., Cote, J., Dent, S., Jenuwien, T., Kouzarides, T., Pillus, L., Reinberg, D., Shi, Y., Shiekhattar, R., Shilatifard, A., Workman, J., and Zhang, Y. (2007) New nomenclature for chromatin-modifying enzymes. *Cell 131*, 633–636.
22. Tang, Y., Holbert, M. A., Wurtele, H., Meeth, K., Rocha, W., Gharib, M., Jiang, E., Thibault, P., Verrault, A., Cole, P. A., and Marmorstein, R. (2008) Fungal Rtt109 histone acetyltransferase is an unexpected structural homolog of metazoan p300/CBP. *Nat. Struct. Mol. Biol. 15*, 738–745.
23. Lin, C., and Yuan, Y. A. (2008) Structural insights into histone H3 lysine 56 acetylation by Rtt109. *Structure 16*, 1503–1510.
24. Stavropoulos, P., Nagy, V., Blobel, G., and Hoelz, A. (2008) Molecular basis for the autoregulation of the protein acetyl transferase Rtt109. *Proc. Natl. Acad. Sci. U.S.A. 105*, 12236–12241.
25. Liu, X., Wang, L., Zhao, K., Thompson, P. R., Hwang, Y., Marmorstein, R., and Cole, P. A. (2008) The structural basis of protein acetylation by the p300/CBP transcriptional coactivator. *Nature 451*, 846–850.
26. Berndsen, C. E., Tsubota, T., Lindner, S. E., Lee, S., Holton, J. M., Kaufman, P. D., Keck, J. L., and Denu, J. M. (2008) Molecular functions of the histone acetyltransferase chaperone complex Rtt109-Vps75. *Nat. Struct. Mol. Biol. 15*, 948–956.
27. Fillingham, J., Recht, J., Silva, A. C., Suter, B., Emili, A., Stagljar, I., Krogan, N. J., Allis, C. D., Keogh, M. C., and Greenblatt, J. F. (2008) Chaperone control of the activity and specificity of the histone H3 acetyltransferase Rtt109. *Mol. Cell. Biol. 28*, 4342–4353.
28. Han, J., Zhou, H., Li, Z., Xu, R. M., and Zhang, Z. (2007) Acetylation of lysine 56 of histone H3 catalyzed by RTT109 and regulated by ASF1 is required for replisome integrity. *J. Biol. Chem. 282*, 28587–28596.
29. Lopes da Rosa, J., Boyartchuk, V. L., Zhu, L. J., and Kaufman, P. D. (2010) Histone acetyltransferase Rtt109 is required for *Candida albicans* pathogenesis. *Proc. Natl. Acad. Sci. U.S.A. 107*, 1594–1599.
30. Pfaller, M. A., and Diekema, D. J. (2007) Epidemiology of invasive candidiasis: A persistent public health problem. *Clin. Microbiol. Rev. 20*, 133–163.
31. Luger, K., Mader, A. W., Richmond, R. K., Sargent, D. F., and Richmond, T. J. (1997) Crystal structure of the nucleosome core particle at 2.8 Å resolution. *Nature 389*, 251–260.
32. Tanaka, Y., Tawaramoto-Sasanuma, M., Kawaguchi, S., Ohta, T., Yoda, K., Kurumizaka, H., and Yokoyama, S. (2004) Expression and purification of recombinant human histones. *Methods 33*, 3–11.
33. Kim, Y., Tanner, K. G., and Denu, J. M. (2000) A continuous, nonradioactive assay for histone acetyltransferases. *Anal. Biochem. 280*, 308–314.
34. Berndsen, C. E., and Denu, J. M. (2005) Assays for mechanistic investigations of protein/histone acetyltransferases. *Methods 36*, 321–331.
35. Berndsen, C. E., Albaugh, B. N., Tan, S., and Denu, J. M. (2007) Catalytic mechanism of a MYST family histone acetyltransferase. *Biochemistry 46*, 623–629.
36. Tanner, K. G., Langer, M. R., and Denu, J. M. (2000) Kinetic mechanism of human histone acetyltransferase P/CAF. *Biochemistry 39*, 15652.
37. Tanner, K. G., Langer, M. R., Kim, Y., and Denu, J. M. (2000) Kinetic mechanism of the histone acetyltransferase GCN5 from yeast. *J. Biol. Chem. 275*, 22048–22055.
38. Sikora, A. L., Frankel, B. A., and Blanchard, J. S. (2008) Kinetic and chemical mechanism of arylamine N-acetyltransferase from *Mycobacterium tuberculosis*. *Biochemistry 47*, 10781–10789.
39. Tanner, K. G., Trievel, R. C., Kuo, M. H., Howard, R. M., Berger, S. L., Allis, C. D., Marmorstein, R., and Denu, J. M. (1999) Catalytic mechanism and function of invariant glutamic acid 173 from the histone acetyltransferase GCN5 transcriptional coactivator. *J. Biol. Chem. 274*, 18157–18160.
40. Han, J., Zhou, H., Li, Z., Xu, R. M., and Zhang, Z. (2007) The Rtt109-Vps75 histone acetyltransferase complex acetylates non-nucleosomal histone H3. *J. Biol. Chem. 282*, 14158–14164.
41. Krogan, N. J., Cagney, G., Yu, H., Zhong, G., Guo, X., Ignatchenko, A., Li, J., Pu, S., Datta, N., Tikuisis, A. P., Punna, T., Peregrin-Alvarez, J. M., Shales, M., Zhang, X., Davey, M., Robinson, M. D., Paccanaro, A., Bray, J. E., Sheung, A., Beattie, B., Richards, D. P., Canadien, V., Lalev, A., Mena, F., Wong, P., Starostine, A., Canete, M. M., Vlasblom, J., Wu, S., Orsi, C., Collins, S. R., Chandran, S., Haw, R., Rilstone, J. J., Gandi, K., Thompson, N. J., Musso, G., St Onge, P., Ghanny, S., Lam, M. H., Butland, G., Altaf-Ul, A. M., Kanaya, S., Shilatifard, A., O'Shea, E., Weissman, J. S., Ingles, C. J., Hughes, T. R., Parkinson, J., Gerstein, M., Wodak, S. J., Emili, A., and Greenblatt, J. F. (2006) Global landscape of protein complexes in the yeast *Saccharomyces cerevisiae*. *Nature 440*, 637–643.
42. Tang, Y., Meeth, K., Jiang, E., Luo, C., and Marmorstein, R. (2008) Structure of Vps75 and implications for histone chaperone function. *Proc. Natl. Acad. Sci. U.S.A. 105*, 12206–12211.
43. Das, C., Lucia, M. S., Hansen, K. C., and Tyler, J. K. (2009) CBP/p300-mediated acetylation of histone H3 on lysine 56. *Nature 459*, 113–117.
44. Berndsen, C. E., and Denu, J. M. (2008) Catalysis and substrate selection by histone/protein lysine acetyltransferases. *Curr. Opin. Struct. Biol. 18*, 682–689.
45. Harris, T. K., and Turner, G. J. (2002) Structural basis of perturbed pKa values of catalytic groups in enzyme active sites. *IUBMB Life 53*, 85–98.
46. Stites, W. E., Gittis, A. G., Lattman, E. E., and Shortle, D. (1991) In a staphylococcal nuclease mutant the side-chain of a lysine replacing valine 66 is fully buried in the hydrophobic core. *J. Mol. Biol. 221*, 7–14.